Appl Nanosci (2017) 7:407–416
DOI 10.1007/s13204-017-0581-z

ORIGINAL ARTICLE

Effective Pb^{2+} removal from water using nanozerovalent iron stored 10 months

M. A. Ahmed[1] · Samiha T. Bishay[2] · Fatma M. Ahmed[1] · S. I. El-Dek[3]

Received: 16 June 2017 / Accepted: 3 August 2017 / Published online: 8 August 2017

Abstract Heavy metal removal from water required reliable and cost-effective considerations, fast separation as well as easy methodology. In this piece of research, nanozerovalent iron (NZVI) was prepared as ideal sorbent for Pb^{2+} removal. The sample was characterized using X-ray diffraction (XRD), high-resolution transmission electron microscope (HRTEM), and atomic force microscope (AFM–SPM). Batch experiments comprised the effect of pH value and contact time on the adsorption process. The same NZVI was stored for a shelf time (10 months) and the batch experiment was repeated. The outcomes of the investigation assured that NZVI publicized an extraordinary large metal uptake (98%) after a short contact time (10 h). The stored sample revealed the same effectiveness on Pb^{2+} removal under the same conditions. The results of the physical properties, magnetic susceptibility, and conductance were correlated with the adsorption efficiency. This work offers evidence that these NZVI particles could be potential candidate for Pb^{2+} removal in large scale, stored for a long time using a simple, green, and cost-effective methodology, and represent an actual feedback in waste water treatment.

Keywords NZVI · Core–shell · AFM · HRTEM · Pb^{2+} removal · Conductance · Magnetic susceptibility

Introduction

Iron nanoparticle was one of the first generation nanoscale environmental technologies. In the past few years, different methods were developed to synthesize iron nanoparticles (Brumfiel 2003; Hassan 2005; Zhang et al. 2015; Su et al. 2016), modify their surface properties (Mahfuz and Ahmed 2005; Karlsson et al. 2004; Rajajayavel and Ghoshal 2015), and improve their efficiency for field delivery and reactions (Liu et al. 2015; Glavee et al. 1995; Khalil et al. 2004; Xu et al. 2005; Zhang et al. 1998; Schrick et al. 2002; Elliott and Zhang 2001). Extensive investigations reported that nanoscale iron particles are effective for the removal of a wide environmental contaminants such as heavy metal ions like As(III), Pb(II), Cu(II), Ni(II), and Cr(VI), chlorinated organic solvents, organochlorine pesticides, some inorganic compounds (Elliott and Zhang 2001; Liu et al. 2005; Alowitz and Scherer 2002; Cao et al. 2005; Kanel et al. 2005), and organic dyes (Alowitz and Scherer 2002; Cao et al. 2005; Kanel et al. 2005).

NZVI is usually reported to have a core–shell structure. The shell contains oxidized iron that is mostly magnetite Fe_3O_4 and often with maghemite (γ-Fe_2O_3) or lepidocrocite (γ-FeOOH) (O'Carroll et al. 2013; Phenrat et al. 2016; Boparai et al. 2013).

Some efforts expanded to examine the specific functions of the metal core and the oxide shell in different remediation systems. More informative knowledge of the core–shell structure and the surface chemistry of NZVI materials can accelerate the development of new applications, especially in the category of inorganic contaminants,

✉ S. I. El-Dek
samaa@psas.bsu.edu.eg; didi5550000@gmail.com

[1] Materials Science Lab (1), Physics Department, Faculty of Science, Cairo University, Giza, Egypt

[2] Physics Department, Faculty of Girls for Arts, Science and Education, Ain Shams University, Cairo, Egypt

[3] Materials Science and Nanotechnology Department, Faculty of Postgraduate Studies for Advanced Sciences, PSAS, Beni-Suef University, Beni-Suef, Egypt

whose treatment typically involves surface-mediated complexation and/or redox transformations (Auffan et al. 2008). Another aspect which has received less attention in the literature is the inevitable reaction of NZVI with water and its effect on the solution and surface chemistry. This point is of particular relevance to the treatment of ionic species including heavy metal ions, because their speciation and reactivity are profoundly dependent on the solution pH.

NZVI corrosion primarily occurred due to the formation of Fe^{2+} or mainly Fe^{3+} species, which can be described as follows (Geng et al. 2009; Uzum et al. 2009; Morgada et al. 2009; Rao et al. 2009):

$$Fe^0 \rightarrow Fe^{2+} + 2e^- \quad (1)$$

$$Fe^{2+} \rightarrow Fe^{3+} + e^- \quad (2)$$

$$Fe^0 \rightarrow Fe^{3+} + 3e^-. \quad (3)$$

If NZVI reacts with ionic heavy metals such as Pb^{2+}, the following reaction takes place

$$Pb^{2+} + Fe^0 \rightarrow Pb^0 + Fe^{2+}. \quad (4)$$

NZVI has engrossed the most consideration from those experts in the art (environmental technicians and scientists) owing to its eclectic applicability and extraordinary removal efficiency. NZVI is branded to be extremely operative at the conversion and detoxification of organic contaminants as well as heavy metals pollutants. The central technical tricky encountered in the handling of such nanoparticles is their high air sensitivity. When unprotected from the air, NZVI is quickly oxidized and misses its high surface reactivity which is mainly its focus advantage. Many procedures have been established to suppress oxidation and protect NZVI during, post-preparation, and at the shelf lifetime (expiration period/storage).

The main goal of this research work is to improve the previous reported methods of preparation NZVI to obtain a sample that could be stored for a long time at normal conditions. Moreover, these nanoparticles are characterized by their physical stability hand in hand with superior chemical catalytic activity. The second essential target is to find out the most suitable situations to utilize this prepared NZVI to remove Pb^{2+} ions from water.

Experimental techniques

Synthesis of NZVI

Modified method was used to prepare PVP–NZVI particles, where the reduction of $FeCl_3$ by $NaBH_4$ using the "bottom–up" method (Boparai et al. 2011) with some modifications is considered. The reduction was carried out by adding droplets of 0.125 M sodium borohydride ($NaBH_4$) aqueous solution to (200 mL) solution of 0.023 M $FeCl_3$ and polyvinyl pyrrolidone (PVP) of 1.3055 g under continuous flow of nitrogen gas with stirring using mechanical stirrer. Ferric ion (Fe^{3+}) was reduced to zerovalent iron (Fe^0) by borohydride according to the following reaction:

$$4Fe^{3+} + 3BH^{4-} + 9H_2O \rightarrow 4Fe^0 \downarrow + 3H_2BO^{3-} + 12H^+ + 6H_2 \uparrow. \quad (5)$$

Black NZVI particles appeared immediately after introducing the first few drops of $NaBH_4$ solution, where the pH value of the reaction was adjusted at ≈8–9. The mixture was stirred for additional 20 min. The precipitated zerovalent iron nanoparticles (NZVI) were separated, washed several times with deoxygenated-deionized water and ethanol, and then stored in thin layer of ethanol. The preparation method in this study is modified than that reported (Boparai et al. 2011) by adding PVP (polyvinyl pyrrolidone). The prepared NZVI does not show visible changes in color which suggested that the PVP used in synthesis procedure protects Fe^0 nanoparticles from air oxidation. In other words, PVP is used as a stabilizer for preparing more physically stable and more chemically reactive NZVI for the removal of metal ions from water as well as it leads to best storage for the prepared NZVI at normal conditions.

X-ray diffraction (XRD) was carried out to assure the formation of the NZVI in a single phase using XPERT-PRO with $CuK_{\alpha 1}$ target ($\lambda = 1.54443$ Å. The particle size and microstructure were examined by HRTEM (Tecnai G20, Super twin, double tilt). The surface topography and roughness profile was examined using atomic force microscope (scanning probe; SPM-9600).

Batch experiment of Pb^{2+} removal

To optimize the conditions of Pb^{2+} removal from water, the following set of experiments was carried out at room temperature. Equivalent weights of NZVI (0.02 g) were added to five similar volumes 10 mL of lead nitrate standard solution (2 ppm), and several drops of ammonia or nitric acid were used to adjust the pH value at (4–8). The investigated solutions were covered by parafilm and shaked well using electric shaker at 250 rpm for 1 h. The atomic absorption measurements were carried out using (PERKIN ELMER A. Analyst 100). The electrical properties of the investigated samples were carried out using LCR meter model HIOKI 3531 (Japan). A quartz cell with two parallel platinum electrodes was especially designed for such purpose.

Results and discussion

Microstructural investigations of fresh NZVI using HRTEM

Figure 1a shows HRTEM micrograph of freshly prepared NZVI sample. Some of the nanoparticles appear agglomerated, due to magnetic and electrostatic attractions. It is worthy noted that the formed black spherical nanoparticles were certainly magnetic and, therefore, attract each other easily. Accordingly, this was a clear evidence of the formation of nanoparticles of zerovalent iron (ZVI). From a closer look using higher magnification, Fig. 1b shows that each single particle appears as a dense black core surrounded by a thin brighter shell of dark gray color. The shell thickness was found from HRTEM to vary significantly between 4 and 6 nm, while the core was occasionally observed as thick as 25 nm and as thin as 9 nm. The core and shell thickness dimensions obtained from HRTEM agree with those previously reported NZVI (Yan et al. 2010). The disordered oxide layer can be partially explained by the ultrafine radius of nanoparticles as well as their agglomeration state. It is noticed from the micrograph that the chains of connected nanoparticles have a continuous oxide shell looking like that previously reported (Liu and Zhang 2014; Wang and Zhang 1997; Ahn et al. 2001).

The uniqueness of our work originated from the extended storage (shelf lifetime) of the obtained NZVI. Herein, after more than 10 months and in the normal atmosphere, there is neither weight loss content nor pronounced microstructural changes in the shell thickness/shape. This originality is remarked in Fig. 2, where the HRTEM of the stored sample of NZVI after more than 10 months shows the identical core–shell with nearly similar dimensions as illustrated in Fig. 1b for the freshly prepared one.

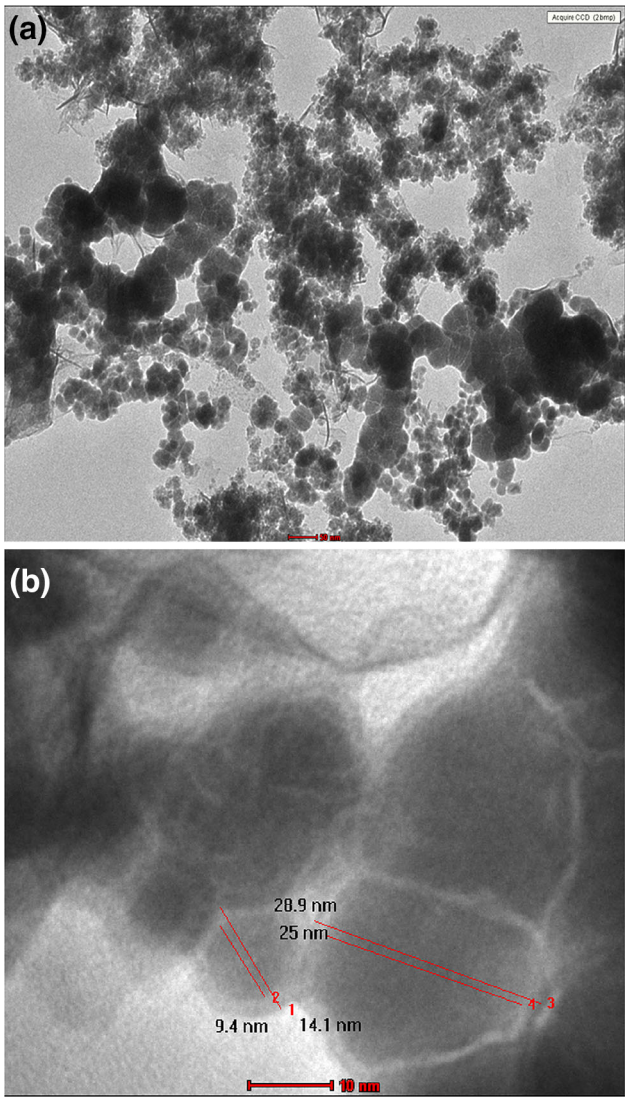

Fig. 1 **a**, **b** HRTEM of the freshly prepared NZVI sample at two different magnifications

Crystal structure and topography of NZVI before and after removal process

XRD characterization of the as-prepared NZVI is shown in Fig. 3a. The peak at $2\theta = 44.9°$ corresponds to the (110) plane indicating the presence of Fe^0; this result is in line with that previously reported (Liang et al. 2014). The broad iron peak implies that the synthesized ZVI is formed in the nanoscale. To calculate the crystallite size, one used

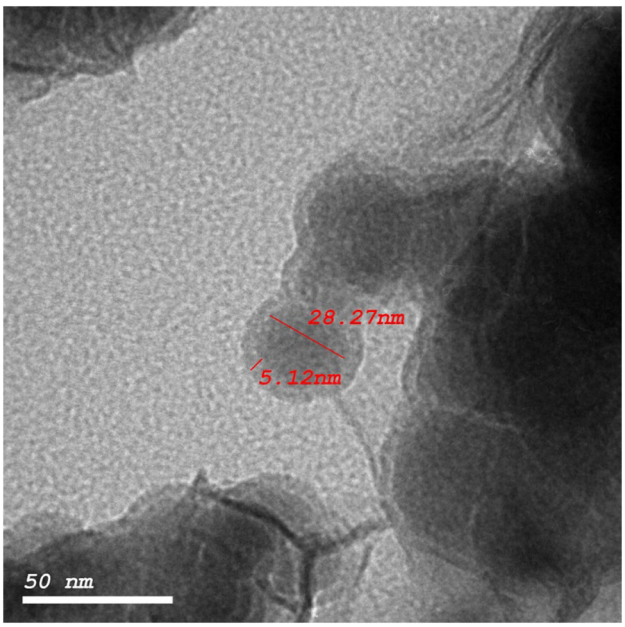

Fig. 2 HRTEM micrograph of NZVI after storage period of 10 months

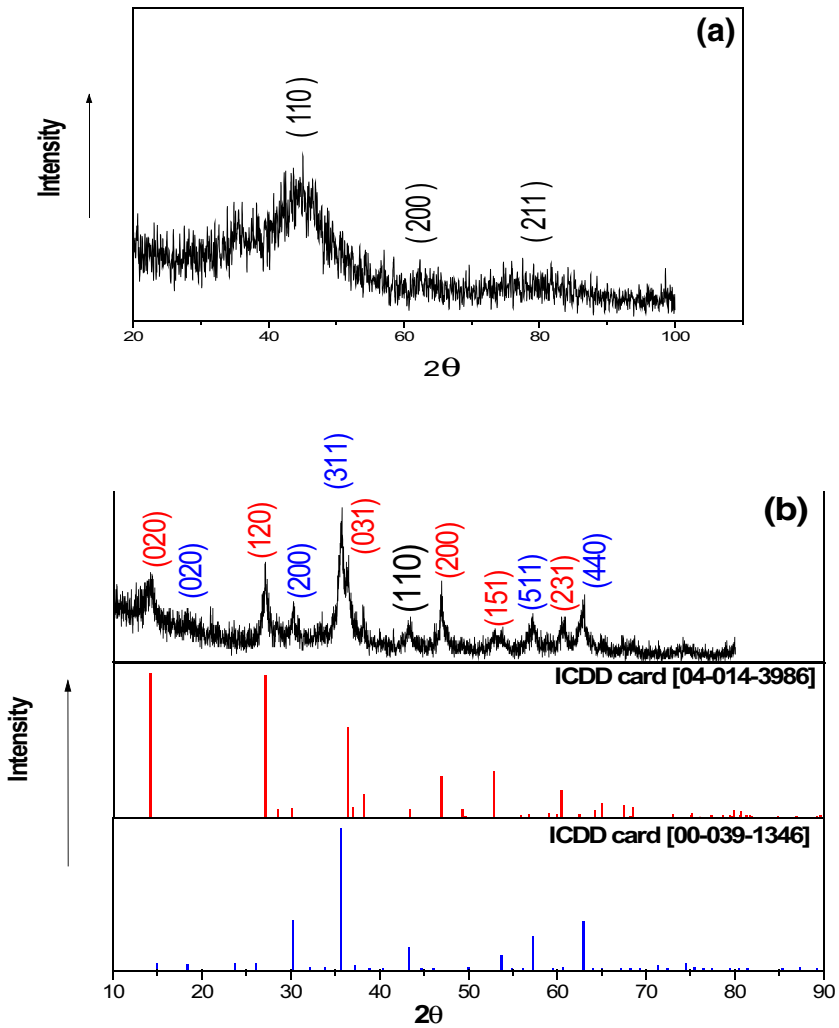

Fig. 3 **a** XRD pattern of the fresh prepared NZVI, **b** XRD pattern of NZVI after Pb^{2+} removal (contact time 1 h)

Scherrer formula (Sun et al. 2007) $L_{hkl} = (0.9\lambda)/\beta_{1/2} \cos\theta$, where L_{hkl} is the crystallite size, λ is the wavelength of CuK_α radiation, $\beta_{1/2}$ is the corrected full-width at half-maximum (FWHM), and θ is the diffraction angle of the strongest peak. The calculated value of the crystallite size of the prepared NZVI is 1 nm. Figure 3b shows the XRD of NZVI after Pb^{2+} removal (at pH 8, contact time 1 h). It is noted that a peak appeared at ($2\theta = 35.631°$) corresponds to the plane (311) of the hematite (Fe_2O_3) according to ICDD card [00-039-1346]. Another peak appeared at ($2\theta = 14.148°$) pointed to the presence of FeO(OH) as identified from ICDD card [04-014-3986] and was indexed as (020). The presence of Fe_2O_3 and FeO(OH) confirmed the redox reactions between $Fe^{(0)}$ and Pb^{2+}, where NZVI acts as a reducing agent (Shu et al. 2007).

Atomic force microscopy was employed to examine surface topography of the synthesized NZVI. The freshly prepared NZVI as shown in Fig. 4a appeared to be more or less distributed in a non-regular manner with large roughness and spherical shape. The size distribution is observed to narrow form the line profile. The surface topographic details resembles to spikes of different heights and widths. Certainly, this will play an important role in the adsorption process. After Pb^{2+} removal (pH 8, 1 h contact time), Fig. 4b, the particles seem to be enlarged. The distribution became broader and the surface could be described as nanoislands with no clear boundaries and lost distinct shells. This reflects that iron corrosion products are formed on the shell and accumulated on the Fe^0 surface as a direct result of the extremely large surface/volume ratio as well as large exposed surface area as it was clear from the ultrafine size of NZVI. Consequently, the particle size gets enlarged after Pb^{2+} removal owing to the reaction products on the nanoparticle surface.

Effect of pH value on the surface charge of NZVI

Surface charge or zeta potential is the major factor determining the mobility of particles in an electric field. The electrostatic repulsion between the nanoparticles depends

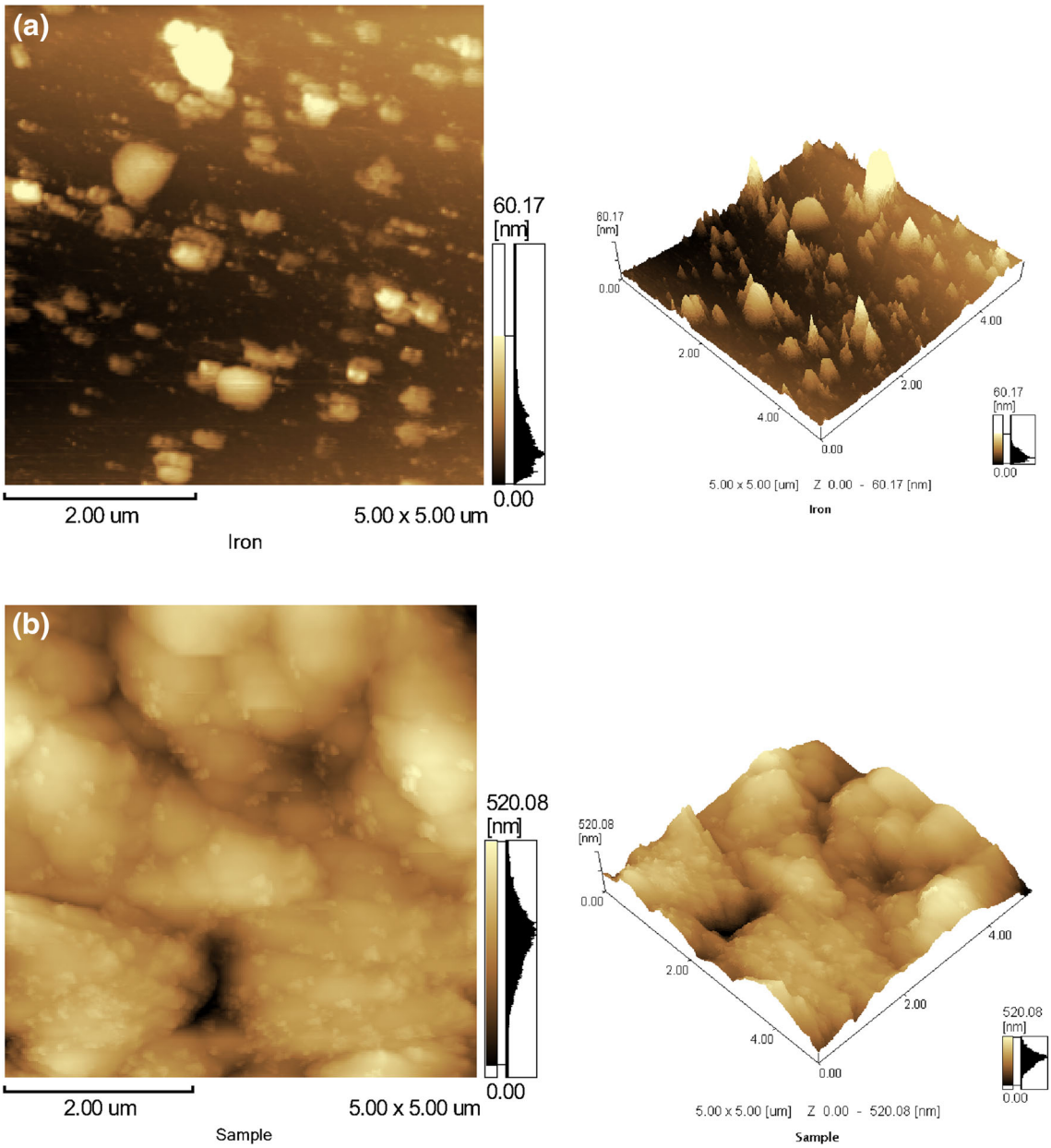

Fig. 4 AFM images for **a** fresh NZVI and **b** NZVI after Pb^{2+} removal (pH 8, contact time 1 h)

on the surface potential determined by zeta potential. The metastable suspension is obtained at the value of zeta potential of ±30 mV (Xi et al. 2010; Larsson et al. 2012). Results in Fig. 5 designate that at low pH value, the particles have a net positive charge, and at higher pH value, a net negative charge was acquired. These results agree well with the reported data (Dickinson and Scott 2010). As demonstrated in Fig. 5, the nanoparticles maintained a surface charge of +15.4 to −30 mV over the pH range of 4–8. When the pH value is less than the iso-electric point (IEP), NZVI exhibits a positive charge. Surface of lead ions carries positive charge and NZVI nanoparticles are negatively charged above the isoelectric point. Therefore, the lead ions will be easily adsorbed on the surface of NZVI.

Effect of pH value on Pb^{2+} removal efficiency and microstructure of NZVI (before and after 10 month storage)

In water, iron oxides possess metal-like or ligand-like coordination properties depending on the solution character (pH). At low pH, iron oxides are positively charged and attract negatively charged ligands (e.g., phosphate, nitrate, chloride, etc). Increasing pH above the iso-electric point (pH ∼8), the surface of the oxide becomes negatively

charged and can form surface complexes with positive cations (Pb^{2+}, Cd^{2+}, and Ni^{2+}).

The adsorption efficiency was calculated from $\{(C_o - C/C_o) \times 100\}$, where C_o is the initial Pb^{+2} concentration and C is its value at the considered condition; the values are reported in Table 1 for the fresh NZVI samples and for those stored for 10 months. The data were collected after similar contact time 1 h. Maximum removal efficiency was recorded at pH 8 which means that NZVI displays double roles (sorbent) and metallic iron (a reductant). The metallic iron was believed to reduce the Pb^{2+} ions and the NZVI reduced the rest of them. The results clarified that the adsorption efficiency of Pb^{2+} ions using NZVI before and after 10 months is approximately the same which means that there is no weight loss in the NZVI. Moreover, one could see that this result in line with the observed microstructure form HRTEM as mentioned above, where core–shell-type nanoparticles with nearly similar dimensions and core/shell thickness ratio were preserved. This is an optimized excellent result after such long time.

Figure 6a–c clarifies the HRTEM micrograph of NZVI after Pb^{2+} adsorption at pH values (6, 7, and 8) and contact time 1 h. Agglomeration of NZVI at the beginning originated from the strong magnetic interactions, although in our case, PVP decreases the electrostatic attraction. Figure 6a shows that pH 6, NZVI core shape is likely to be still small as compared with that of the fresh prepared sample, Fig. 1a. Correspondingly, no clear change in the size could be detected at pH 7, Fig. 6b. This is back to the small adsorption efficiency achieved at this pH value. Figure 6c, pH 8, shows that the core–shell structure disappeared completely as a result of the highest adsorption efficiency of lead ions on the surface of NZVI that took place, as discussed in Fig. 4b. Furthermore, from Fig. 6a–c, we conclude that the particle size of NZVI after lead adsorption becomes larger than that before, as shown in Fig. 4a, b.

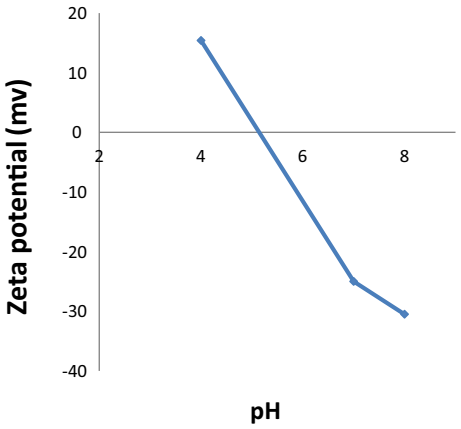

Fig. 5 Zeta potential of NZVI as a function of pH value

Table 1 Removal efficiency percentage of Pb^{+2} using NZVI after contact time 1 h at different pH values for the freshly prepared sample and that stored 10 months

pH	Removal efficiency (%) for (2 mg Pb^{+2}/1 g NZVI)	
	NZVI (fresh sample)	NZVI (stored 10 months)
4	85.3	–
5	88.2	–
6	91.9	91.4
7	83.6	83.2
8	99.8	98.9

Effect of contact time on the Pb^{2+} removal efficiency

The adsorption efficiency of NZVI in lead removal at pH 8 is certainly time dependent. The obtained results of Fig. 7 clarify that, using only 1.0 g/L of our prepared NZVI, the adsorption efficiency reached 95% after 1 h and complete (100%) uptake is after 24 h. This is an applicable result in fast water detoxification, as one can use these prepared NZVI to remove large percentage of Pb in a very short contact time. Here, this result was due to the number of available active sites for adsorption owing to the excellent specific surface area of the samples.

Study of the electrical conductance and its correlation with removal efficiency

Figure 8 represents the dependence of the room temperature electrical conductance (G) of NZVI on pH values. The comparison between Table 1 and Fig. 8 pointed to the matching between the adsorption efficiency and the conductance of the NZVI. This is interpreted as the lead adsorption which is accompanied by an increase in the maghemite shell, as discussed above in XRD data, Fig. 3a, b. From another point of view, the lead adsorption by NZVI is accompanied by liberation of electron charge carriers as explained before.

Figure 9 represents the frequency dependence of the conductance of NZVI at different pH values after 1 h contact time. The results from this figure clarify that a similar variation of the conductance with the applied frequency was obtained at all pH values. The conduction and polarization processes in nanoparticles are certainly depending on many factors including electrical double layer at the mineral/water interface, applied frequency, and temperature. For NZVI, these physical properties are impacted by the charge transfer and valence exchange for the existing iron ions during the redox reaction across the interface. Herein, the interfacial polarization is highly pronounced and Maxwell–Wagner type plays a significant

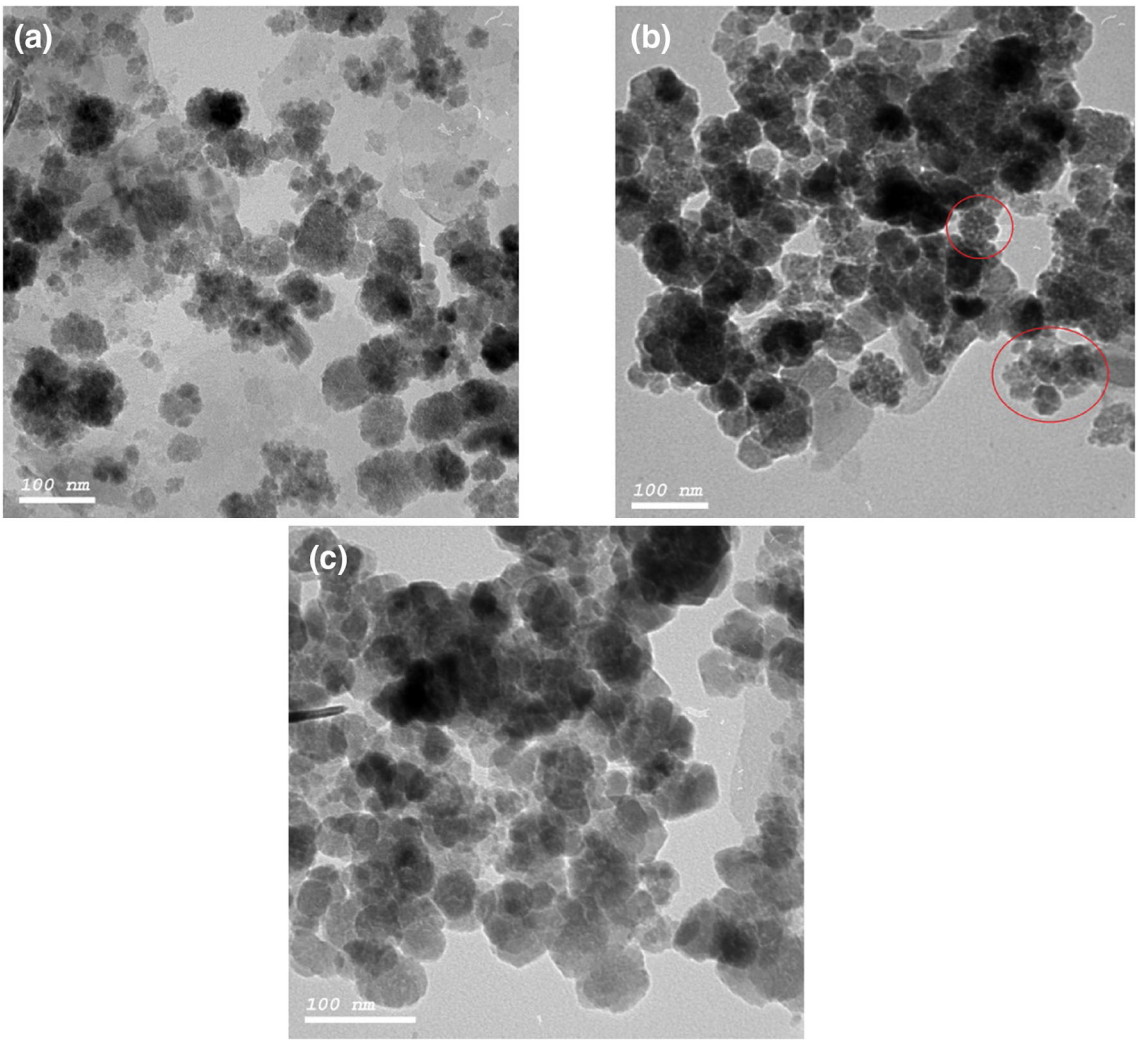

Fig. 6 HRTEM micrograph for NZVI after Pb^{2+} adsorption at different pH values, **a** pH 6, **b** pH 7, and **c** pH 8

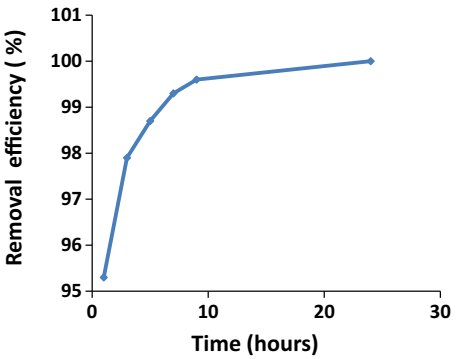

Fig. 7 Dependence of lead ion removal efficiency on contact time at pH 8 using NZVI

role especially at elevated temperatures. Since one assumed that the interface between NZVI and water takes the upper hand in controlling electrical properties,

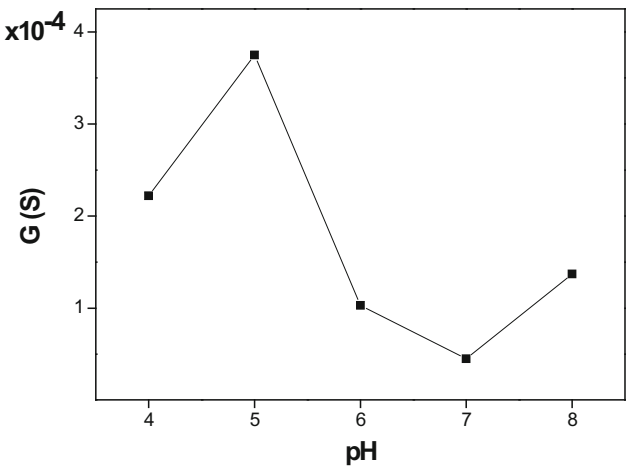

Fig. 8 Effect of pH value on the conductance of Pb^{2+} nitrate solution with NZVI after 1 h at room temperature at 1 MHz

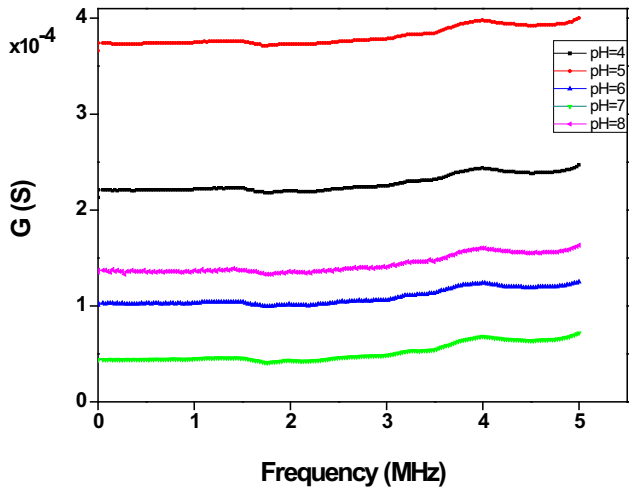

Fig. 9 Effect of frequency on the conductance of lead nitrate solution with NZVI at different pH values

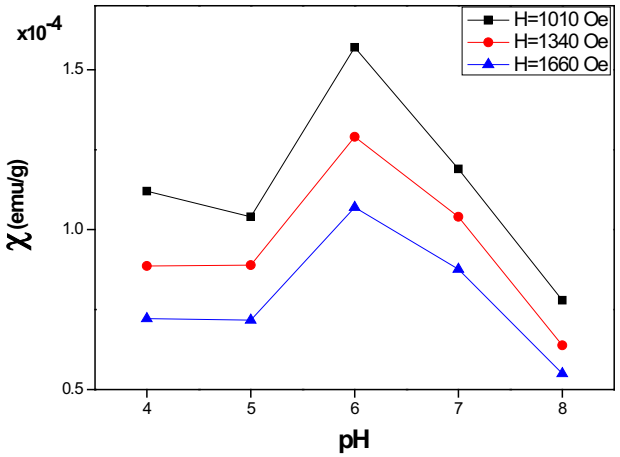

Fig. 10 Magnetic susceptibility of NZVI at different pH values at room temperature as a function of magnetic field intensity

therefore, physico-chemical studies here must be highlighted represented in the surface area. The latter is inversely proportional to the crystallite size as the relation is depicted from

$$S = \frac{\text{surface area}}{\text{Mass}} \text{ (Sun et al. 2006)} \quad (6)$$

$$S = \frac{6}{\rho L} \quad (7)$$

where ρ is the density and taken here (7800 kg/m^3) for iron and L is the crystallite size (particle diameter assuming spherical shape) as obtained from XRD. For our NZVI, the calculated surface area is 76.92 $\times$ 10^4 or 769 m^2/g which is a surprising result and exceedingly larger than obtained earlier (Cornell 2003). The obtained surface area is six times more than that obtained and reported by Sun et al. (2006).

Zerovalent iron, Fe^0, has been renowned as an effective electron donor irrespective of its particle size. This is supported by the standard reduction potential (E^0) of −440 mV for the following half-reaction between the $Fe^{2+/}Fe^0$ pair:

$$Fe^{2+} + 2e^- \rightarrow Fe^0. \quad (8)$$

In the water environment, the predominant electron receptors are water and to some extent residual dissolved oxygen:

$$\begin{aligned} Fe^0_{(s)} + 2H_2O_{(aq)} &\rightarrow Fe^{2+}_{(aq)} + H_{2(g)} + 2OH^-_{(aq)} \\ 2Fe^0_{(s)} + 4H^+_{(aq)} + O_{2(aq)} &\rightarrow 2Fe^{2+}_{(aq)} 2H_2O_{(l)}. \end{aligned} \quad (9)$$

Herein, the conductivity originated from the number of electrons liberated during redox reaction as well as their mobility. In other words, the predominant effect on the conduction mechanism is the remediation process (the medium alkalinity and/or acidity) rather than the applied frequency. This is evidenced by the change in G with pH values that is observed to be more significant than that produced by scanning over the whole frequency range (0.4–5 MHz).

Study of the magnetic susceptibility of NZVI at different pH values

Figure 10 illustrates the dependence of the room temperature magnetic susceptibility χ at different pH of the solution of NZVI after 1 h contact as a function of magnetic field intensity. The values of the magnetic susceptibilty decreased as the magnetic field increased as the general trend of magnetic materials (Ahmed et al. 2013). The variation of χ with the pH value is interpreted depending on the obtained HRTEM micrograph, Fig. 6a–c, and the adsorption efficiency, Table 1. It is noted that, the smallest magnetic susceptibility values are attained at pH 8, this corresponds to high adsorption efficiency, i.e., where the thickness of the iron oxide gets enlarged. This means that the predominant factor affecting on the magnetic susceptibility is the iron oxide shell and the ZVI core has a minor contribution. Moreover, Fig. 10 shows that the largest χ is obtained for the solution at pH 6. This is back to, at this pH value, the shell thickness of the NZVI possess small value, as appeared in Fig. 6a. Here, the importance of the magnetic properties of the NZVI is highlighted in how the material after adsorption could be recovered and easily removed from water after decontamination process using external magnetic field.

Compliance with ethical standards

Funding This study was not funded by any grant.

Conflict of interest The authors declare that they have no conflict of interest.

References

Ahmed MA, Helmy N, El-Dek SI (2013) Innovative methodology for the synthesis of Ba-M hexaferrite $BaFe_{12}O_{19}$ nanoparticles. Mater Res Bull 48(9):3394–3398

Ahn SY, Oh JH, Sohn KH (2001) Mechanistic aspects of nitrate reduction by $Fe^{(0)}$ in water. J Korean Chem Soc 45:395–398

Alowitz MJ, Scherer MM (2002) Kinetics of nitrate, nitrite, and Cr(VI) reduction by iron metal. Environ Sci Technol 36:299–306

Auffan M, Achouak W, Rose E, Roncato M-A, Chanéac C, Waite DT, Masion A, Woicik JC, Wiesner MR, Bottero J-Y (2008) Relation between the redox state of iron-based nanoparticles and their cytotoxicity toward *Escherichia coli*. Environ Sci Technol 42:6730–6735

Boparai HK, Joseph M, O'Carroll DM (2011) Kinetics and thermodynamics of cadmium ion removal by adsorption onto nano zerovalent iron particles. J Hazard Mater 186(1):458–465

Boparai HK, Joseph M, O'Carroll DM (2013) Cadmium ($Cd^{(2+)}$) removal by nano zerovalent iron: surface analysis, effects of solution chemistry and surface complexation modeling. Environ Sci Pollut Res Int 20(9):6210–6221

Brumfiel G (2003) A little knowledge…. Nature 424:246–248

Cao J, Elliott D, Zhang W-X (2005) Perchlorate reduction by nanoscale iron particles. J Nanopart Res 7(4–5):499–506

Cornell RM (2003) U. S., The iron oxide, structure, properties, interactions, occurrence and uses. Wiley Vich, New York, p 2003

Dickinson M, Scott TB (2010) The application of zero-valent iron nanoparticles for the remediation of a uranium-contaminated waste effluent. J Hazard Mater 178(1–3):171–179

Elliott DW, Zhang W-X (2001) Field assessment of nanoscale bimetallic particles for groundwater treatment. Environ Sci Technol 35:4922–4926

Geng B, Jin Z, Li T, Qi X (2009) Preparation of chitosan-stabilized Fe(0) nanoparticles for removal of hexavalent chromium in water. Sci Total Environ 407(18):4994–5000

Glavee GN, Christopher KJ, Sorensen CM, Hadjipanay GC (1995) Chemistry of borohydride reduction of iron(I1) and iron(II1) ions in aqueous and nonaqueous media. formation of nanoscale Fe, FeB, and Fe2B powders. Inorg Chem 34:28–35

Hassan MHA (2005) Small things and big changes in the developing world. Science 309:65–66

Kanel SR, Manning B, Charlet L, Choi H (2005) Removal of arsenic(III) from groundwater by nanoscale zero-valent iron. Environ Sci Technol 39:1291–1298

Karlsson MNA, Deppert K, Wacaser BA, Karlsson LS, Malm JO (2004) Size-controlled nanoparticles by thermal cracking of iron pentacarbonyl. Appl Phys A 80(7):1579–1583

Khalil H, Mahajan D, Rafailovich M, Gelfer M, Pandya K (2004) Synthesis of zerovalent nanophase metal particles stabilized with poly(ethylene glycol). Langmuir: ACS J Surf Colloids 20:6896–6903

Larsson M, Hill A, Duffy J (2012) Suspension stability; why particle size, zeta potential and rheology are important. Annu Trans Nordic Rheol Soc 20:209–214

Liang W, Dai C, Zhou X, Zhang Y (2014) Application of zero-valent iron nanoparticles for the removal of aqueous zinc ions under various experimental conditions. PLoS One 9(1):e85686

Liu A, Zhang W (2014) Fine structural features of nanoscale zero-valent iron characterized by spherical aberration corrected scanning transmission electron microscopy (Cs-STEM). Analyst 139:4512–4518

Liu Y, Majetich SA, Tilton RD, Sholl DS, Lowry GV (2005) TCE dechlorination rates, pathways, and efficiency of nanoscale iron particles with different properties. Environ Sci Technol 39:1338–1345

Liu Y, Wang Q, Zhang Y, Ni BJ (2015) Zero valent iron significantly enhances methane production from waste activated sludge by improving biochemical methane potential rather than hydrolysis rate. Sci Rep 5:8263

Mahfuz MU, Ahmed KM (2005) A review of micro-nano-scale wireless sensor networks for environmental protection: prospects and challenges. Sci Technol Adv Mater 6(3–4):302–306

Morgada ME, Levy IK, Salomone V, Farías SS, López G, Litter MI (2009) Arsenic(V) removal with nanoparticulate zerovalent iron: effect of UV light and humic acids. Catal Today 143(3–4):261–268

O'Carroll D, Sleep B, Krol M, Boparai H, Kocur C (2013) Nanoscale zero valent iron and bimetallic particles for contaminated site remediation. Adv Water Resour 51:104–122

Phenrat T, Thongboot T, Lowry GV (2016) Electromagnetic induction of zerovalent iron (ZVI) powder and nanoscale zerovalent iron (NZVI) particles enhances dechlorination of trichloroethylene in contaminated groundwater and soil: proof of concept. Environ Sci Technol 50(2):872–880

Rajajayavel SR, Ghoshal S (2015) Enhanced reductive dechlorination of trichloroethylene by sulfidated nanoscale zerovalent iron. Water Res 78:144–153

Rao P, Mak MS, Liu T, Lai KC, Lo IM (2009) Effects of humic acid on arsenic(V) removal by zero-valent iron from groundwater with special references to corrosion products analyses. Chemosphere 75(2):156–162

Schrick B, Blough JL, Jones AD, Mallouk TE (2002) Hydrodechlorination of trichloroethylene to hydrocarbons using bimetallic nickel-iron nanoparticles. Chem Mater 14:5140–5147

Shu HY, Chang MC, Yu HH, Chen WH (2007) Reduction of an azo dye acid black 24 solution using synthesized nanoscale zerovalent iron particles. J Colloid Interface Sci 314(1):89–97

Su Y, Adeleye AS, Huang Y, Zhou X, Keller AA, Zhang Y (2016) Direct synthesis of novel and reactive sulfide-modified nano iron through nanoparticle seeding for improved cadmium-contaminated water treatment. Sci Rep 6:24358

Sun YP, Li XQ, Cao J, Zhang WX, Wang HP (2006) Characterization of zero-valent iron nanoparticles. Adv Coll Interface Sci 120(1–3):47–56

Sun Y-P, Li X-Q, Zhang W-X, Wang HP (2007) A method for the preparation of stable dispersion of zero-valent iron nanoparticles. Colloids Surf A 308(1–3):60–66

Uzum C, Shahwan T, Eroglu A, Hallam K, Scott T, Lieberwirth I (2009) Synthesis and characterization of kaolinite-supported zero-valent iron nanoparticles and their application for the removal of aqueous Cu^{2+} and Co^{2+} ions. Appl Clay Sci 43(2):172–181

Wang CB, Zhang WX (1997) Synthesizing nanoscale iron particles for rapid and complete dechlorination of TCE and PCBs. Environ Sci Technol 31:2154–2156

Xi Y, Mallavarapu M, Naidu R (2010) Reduction and adsorption of Pb^{2+} in aqueous solution by nano-zero-valent iron—a SEM, TEM and XPS study. Mater Res Bull 45(10):1361–1367

Xu J, Dozier A, Bhattacharyya D (2005) Synthesis of nanoscale bimetallic particles in polyelectrolyte membrane matrix for reductive transformation of halogenated organic compounds. J Nanopart Res 7(4–5):449–467

Yan W, Herzing AA, Kiely CJ, Zhang WX (2010) Nanoscale zero-valent iron (nZVI): aspects of the core–shell structure and reactions with inorganic species in water. J Contam Hydrol 118(3–4):96–104

Zhang W, Wang C, Lien H (1998) Treatment of chlorinated organic contaminants with nanoscale bimetallic particles. Catal Today 40:387–395

Zhang Y, Chen W, Dai C, Zhou C, Zhou X (2015) Structural evolution of nanoscale zero-valent iron (nZVI) in anoxic $Co^{(2+)}$ solution: interactional performance and mechanism. Sci Rep 5:13966